Seatific Journal

Volume 5 | Issue 1 Article 2

2025

Analysis of the performance of two moving mesh methods applied to semi-submerged structures with a rotational DOF

Yanca Da CUNHA PEREIRA
School of Engineering, Federal University of Rio Grande, Rio Grande, RS, Brazil

Paulo Roberto De FREITAS TEIXEIRA
School of Engineering, Federal University of Rio Grande, Rio Grande, RS, Brazil, pauloteixeira@furg.br

Eric DIDIER
Department of Hydraulics and Environment, National Civil Engineering Laboratory, Lisbon, Portugal

Recommended Citation

PEREIRA, Yanca Da CUNHA; TEIXEIRA, Paulo Roberto De FREITAS; and DIDIER, Eric (2025) "Analysis of the performance of two moving mesh methods applied to semi-submerged structures with a rotational DOF," *Seatific Journal*: Vol. 5: Iss. 1, Article 2.
https://doi.org/10.29187/2792-0771.1034
Available at: https://commons.yildiz.edu.tr/seatific/vol5/iss1/2

Seatific, Vol. 5, Issue. 1, pp. 11–21, June 2025

Seatific Journal
https://seatific.yildiz.edu.tr
DOI: https://doi.org/10.29187/2792-0771.1034

Research Article

Analysis of the performance of two moving mesh methods applied to semi-submerged structures with a rotational DOF

Yanca Da CUNHA PEREIRA[1], Paulo Roberto De FREITAS TEIXEIRA[1*], Eric DIDIER[2]

[1]*School of Engineering, Federal University of Rio Grande, Rio Grande, RS, Brazil*
[2]*Department of Hydraulics and Environment, National Civil Engineering Laboratory, Lisbon, Portugal*

ARTICLE INFO

Article history
Received: October 24, 2024
Revised: December 12, 2024
Accepted: January 17, 2025

Key words:
CFD; moving mesh; pendulor device; rotational DOF; wave energy

ABSTRACT

Numerical analyses of a buoy with a rotational DOF and a Pendulor-type wave energy converter subjected to incident regular waves are carried out. The ANSYS Fluent® software, based on the Reynolds Averaged Navier-Stokes equations, is used for the free surface flow simulations. The k–ω SST turbulence model and the Volume of Fluid technique, to consider the two-phase flow, composed of air and water, are employed. The performance of two moving mesh methods are analyzed, the dynamic mesh (DM) and sliding mesh (SM) methods. The numerical results of the free decay test and the incident wave over the buoy, obtained by both moving mesh methods, show very good agreement with experimental ones. Besides, both moving methods have similar results in the case of the incident wave over the Pendulor device. The DM method required from 1.29 to 1.44 times the computational time of the SM method. Therefore, both methods have good accuracy to deal with problems that involve semi-submerged structures with a rotational DOF in a plane. However, the SM method has the advantage of requiring less computational time.

Cite this article as: Pereira YD, Teixeira PRF, Didier E. Analysis of the performance of two moving mesh methods applied to semi-submerged structures with a rotational DOF. Seatific 2025;5:1:11–21.

1. INTRODUCTION

The interaction between waves and submerged or floating structures with rigid body movements is an important phenomenon in engineering. It can be emphasized studies about wave effects on ships and on some types of wave energy converters.

Different from other engineering cases, the numerical simulation of the interaction of waves with a moving structure inserted into a tank has some particularities, such as the need to avoid the re-reflection of the wave maker and the radiation boundaries into the tank; the implementation of an adequate technique to deal with a mesh that follows the movement of the boundaries of the moving structure and, simultaneously, maintain the fixed boundaries; the preservation of the accuracy of the solution in the region around the free surface, which may be subjected to the breaking phenomenon.

There are different methodologies to treat the body movements in numerical wave flumes or tanks. In the immersed boundary method or cut-cell method (Causon et al., 2000), the body is cut out of the background mesh leaving partially cut cells. Body motion is taken into account by repeating the cutting procedure with the new boundary conditions. Westphalen et al. (2014) compared the finite volume based Euler equation model using this moving mesh method with a meshless Smoothed Particle Hydrodynamics (SPH) method in numerical simulations of the interaction between regular waves and a horizontal cylinder.

*Corresponding author.
*E-mail address: pauloteixeira@furg.br

In the overset grid or Chimera method, two meshes internally statics with fixed mesh connectivity have relative movement and there is an interpolation of the solution between meshes (Benek et al., 1983). The large body displacements can occur without changing the mesh topology. The authors which used this methodology are Benites-Munoz et al. (2024) using the source code Open FOAM, Luan et al. (2024) and Elhanafi et al. (2017) using the STAR-CCM+ software, among others.

In the fast-fictitious-domain method (Sharma and Patankar, 2005), the moving bodies are represented by the fractional cell volumes and areas on cell sides, in a similar manner to the VoF method for tracking the free surface elevation, allowing large amplitude body motion. Ghasemi et al., (2017), Anbarsooz et al. (2014), among others, used this method.

The body or boundary fitted approach, which adjusts the position of the body surface at each instant, is the most used methodology in the cases of body movement. There are two techniques of the mesh movement which may be applied in this type of approach: Dynamic Mesh (DM) and Sliding Mesh (SM) (Windt et al., 2018).

In the DM method, the mesh is deformed with the lowest possible distortion. The computational efficiency of the method is good; however, the larger the element distortion, the higher the numerical errors are. In the case of high element distortions, the remeshing technique can be used; however, this procedure introduces errors due to interpolations between the new and old meshes and increase the computational time. Several authors have used this methodology, such as Wei et al. (2024) with the multi-phase solver interFoam code, Amini et al. (2023) with the Flow3D software, and Li and Teng (2021) and Penalba et al. (2018) with the package OpenFOAM, among others.

In the SM method, a mesh around the body follows its movement and a static mesh is connected to the moving mesh through the interface of the meshes. In this interface, the mesh is non-conform and the variables are interpolated at each time step, which can cause some numerical errors. Analyses carried out by Ko et al. (2020) and Schmitt and Elsaesser (2015) with the OpenFOAM, and Wei et al. (2015) with the ANSYS Fluent® software used this moving body method.

This study aims to analyze the accuracy and computational time of two moving mesh techniques, SM and DM, for two cases of structures with one Degree Of Freedom (DOF) of rotation subjected to the incident regular waves. The numerical simulations are carried out by using the ANSYS Fluent® software (2016), which is based on the Navier-Stokes equations. The first investigation consists of a buoy studied by Jung (2004) through experiments at small scale. Two cases are studied in a wave flume with a horizontal bottom: a) the roll motion in free decay test; and b) the incident regular wave over the buoy. The second analysis is about a Pendulor-type wave energy converter (Gunawardane et al., 2016). This device has a flap that oscillates around an axis due to the action of waves and coupled hydraulic cylinders transmit mechanical energy to an electric energy conversion system.

2. MATERIALS AND METHODS

The governing equations of the flow and the rigid body motion of a structure with a rotational DOF are shown. Besides, the methodologies used in ANSYS Fluent® for the numerical simulations are described.

2.1. Mathematical model

The governing equations of the flow are composed of the continuity and the momentum equations (Schilichting, 1979), in which the water and air are fluids considered to be incompressible:

$$\frac{\partial u_i}{\partial x_i}=0 \tag{1}$$

$$\frac{\partial(\rho u_i)}{\partial t}+\frac{\partial(\rho u_i u_j)}{\partial x_j}=-\frac{\partial p}{\partial x_i}+\rho g_i+\frac{\partial \tau_{ij}}{\partial x_j} \tag{2}$$

$$\tau_{ij}=\mu\left(\frac{\partial u_i}{\partial x_j}+\frac{\partial u_j}{\partial x_i}\right)-\frac{2}{3}\mu\frac{\partial u_k}{\partial x_k}\delta_{ij} \tag{3}$$

where i, j, k = 1, 2, u_i are the velocity components, t is the time, p is the pressure, ρ is the specific mass, and gi the gravity acceleration components. τ_{ij} is the viscous stress tensor and μ is the fluid viscosity. The RANS equations (Reynolds-Averaged Navier-Stokes) are obtained by the decomposition of the instantaneous velocity and the pressure of the Navier-Stokes equations into average and fluctuating components and integrating these equations over time. The turbulence of the flow is considered by means of the Reynolds stress tensor according to the Boussinesq hypothesis. In this study, the turbulence model, which allows closing the equation system and relating the Reynolds stress tensor with the variables of the flow, is the k–ω SST (Shear Stress Transport) turbulence model (Menter, 1965).

The free surface movement is defined by using the VoF (Volume of Fluid) technique proposed by Hirt and Nichols (1981), which consists of identifying the free surface position through the volume fraction, f, which is null for the air, 1 for the water and 0.5 for the free surface position. The volume fraction transport equation is given by

$$\frac{\partial f}{\partial t}+u_j\frac{\partial f}{\partial x_j}=0 \tag{4}$$

The numerical model of ANSYS Fluent® (2016) is used to develop the 2D wave flume and the semi-submerged moving body, whose sketch is shown in Figure 1. The volume finite technique (Perić and Ferzinger, 1997), in which the variables are defined at the center of the mesh cells, is applied to solve the RANS and VoF equations.

The time integration is carried out by using an implicit formulation and a first-order time discretization.

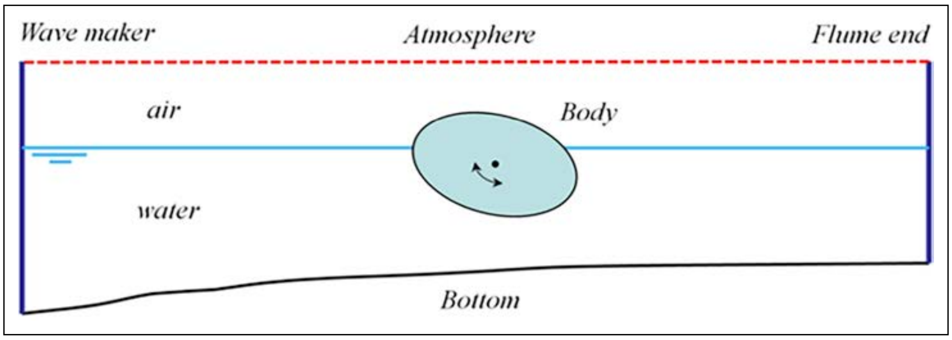

Figure 1. Sketch of cases with semi-submerged bodies with a rotational DOF.

DOF: Degree Of Freedom.

The SIMPLEC (Semi-Implicit Method for Pressure Linked Equations-Consistent) algorithm is used for the coupling of pressure and velocity. The convective terms of the momentum equations are determined by the third-order MUSCL (Monotonic Upstream-Centered Scheme for Conservation Laws) scheme and the second-order UPWIND is used for the equations of the k–ω SST turbulence model. The pressure is determined by PRESTO! (PREssure STaggering Option) scheme, which is classically used to model the wave propagation in ANSYS Fluent® (2016). The relaxation factors are 0.3 for the pressure, 0.7 for the momentum, and 0.8 for the turbulence kinetic energy (k) e the specific dissipation rate (ω). In the VoF method, the explicit formulation is used for the volume fraction and the Geo-Reconstruct scheme is used for the air-water interface.

The following boundary conditions are imposed: atmospheric pressure on the top of the flume; walls and bottom with no-slip conditions; and k = 10^{-6} m^2/s^2 and ω=1 s^{-1} on the wave maker, the top of the flume, and the end of the flume (Lin e Liu, 1998; Elhanafi et al., 2016). The free surface level at rest, null velocity components, the hydrostatic pressure on the water, and the atmospheric pressure on the air are initial conditions.

2.2. The rotational DOF equation

A structure with a rotational DOF in a plane subjected to a moment is governed by the equation (Fig. 1):

$$I\ddot{\theta}+M_f+M_p=M_h \tag{5}$$

where $\ddot{\Theta}$ is the angular acceleration of the structure, I is the mass moment of inertia in relation to the hinge, M_f is the moment caused by the reaction forces of the system coupled to the structure due to the friction and/or forces imposed by external devices, M_p is the moment due to the structure weight, and M_h is the hydrodynamic moment imposed by the flow, caused by the pressure, the viscous stress and the buoyance forces applied to the surface of the structure.

2.3. Moving mesh methods

In this study, two different methods of the moving mesh are used: the Sliding Mesh (SM) and the Dynamic Mesh (DM), which are briefly described below.

In the SM method, the interfaces between the adjacent zones of the mesh slip each other along the time. Therefore, the intersections between the interfaces are updated each time step. In this study, the moving zone is circular and follows the rotation of the circumference around its center, which slips over the circumference that belongs to the fixed external zone of the domain. Therefore, in this interface, the mesh is non-conform.

The movement of the moving mesh zone is governed by the rigid body rotation of the moving boundary around the circumference center. A six DOF system is solved at each instant according to the moving body Law. The moving body equation is imposed by a specific function named DEFINE_SDOF_PROPERTIES in ANSYS Fluent®, which is wrote in an UDF (User Defined Functions). The moving body equation of a system is calculated by using an implicit updated.

In the DM method, the smoothing method is used to deform the mesh along the time in a zone around the moving body. The mesh nodes are displaced to follow the body movement and, at the same time, provide a better geometric quality of the cells. The diffusion-based smoothing technique is employed to move the nodes, which is governed by the diffusion equation given by:

$$\nabla.(\gamma\ \nabla\vec{u})=0 \tag{6}$$

where $\vec{u}$ is the mesh node velocity and γ is the diffusion coefficient, which is calculated as a function of the distance between boundaries, as follows

$$\gamma=\frac{1}{d^{\alpha}} \tag{7}$$

where d is the normalized distance between boundaries and α is the diffusion parameter, whose value used in this study is 1.5, which is recommended by the ANSYS Fluent® manual for body rotations.

Equation (6) is discretized by the finite element method and allows obtainig the mesh node velocity. Therefore, the node positions are updated at each instant as follows:

$$\vec{x}_{t+\Delta t}=\vec{x}_t+\vec{u}\,\Delta t \tag{8}$$

The mesh cell quality can be evaluated by an orthogonal quality index which varies from 0 to 1, in which the higher the value, the better the cell quality (ANSYS, 2015).

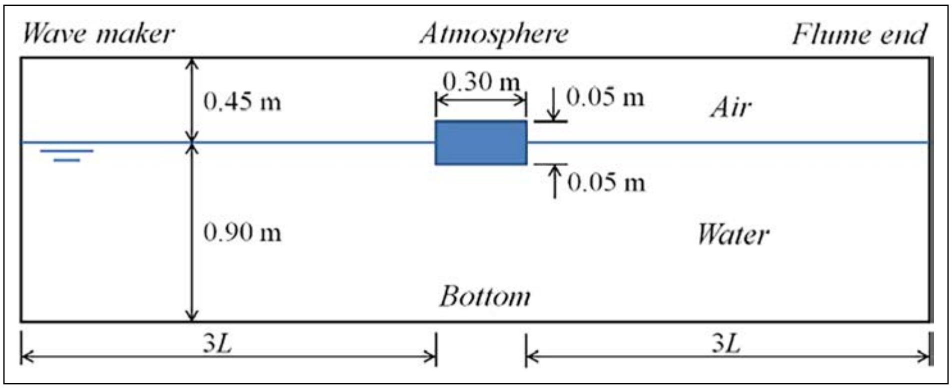

Figure 2. Sketch of the computational domain to the buoy case.

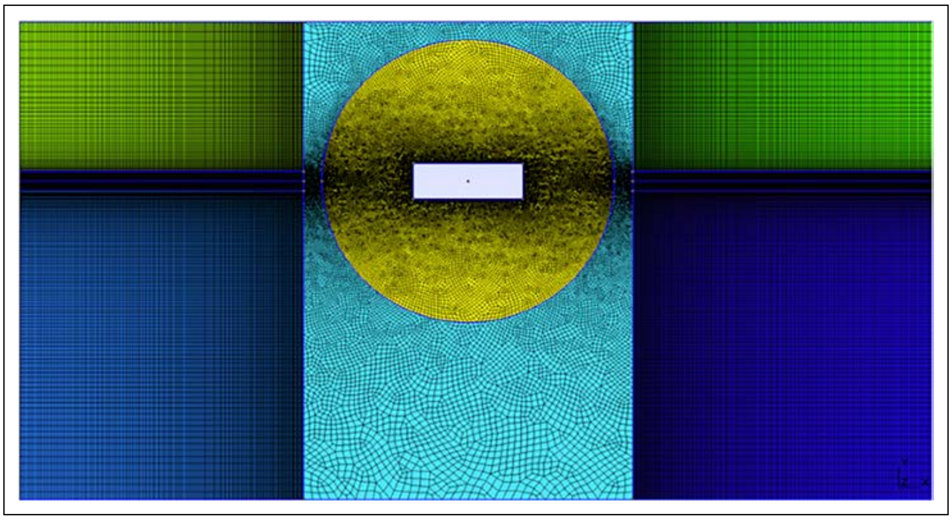

Figure 3. Mesh around the buoy.

3. RESULTS AND DISCUSSION

3.1. Buoy

This case is based on the Jung (2004) experiments, which investigated the behavior of a semi-submerged hexahedral buoy in a flume 0.9 m deep and 0.9 m wide. The buoy has only the rotational DOF around the gravity center (mass moment of inertia I=0.236 kg.m^2), which is at the free surface at the rest. The buoy has a height and length of 0.1 and 0.3 m, respectively, which fills all the width of the flume and, consequently, allows considering a 2D flow behavior. In this study, two cases are analyzed: the free rotation decay from an inclination of 15°, which identifies its natural oscillation period; and the interaction between the buoy and an incident regular wave with a period T=0.93 s and a height H=0.027 m.

Figure 2 shows a sketch of the computational domain, in which the wave flume is 6L + 0.3 m long (L=1.35 m), with the buoy located at the center of the flume. The friction of the moving parts due to the buoy rotation is considered as a viscous friction, in which the damping coefficient of c = 0.3056 Nms/rad is adopted (Calderer et al., 2014).

In the case of the free decay test, the left and right boundaries are considered vertical walls, whereas, in the case of the incident wave over the buoy, there is a static wave maker on the left boundary and a radiation boundary on the right. At the wave maker, velocity components and the volume fraction are imposed, corresponding to the characteristics of the incident wave, by using the active absorption technique (Didier et al., 2017; Teixeira et al., 2017; Didier and Teixeira, 2022). At the radiation boundary, the active absorption technique is also applied to avoid the wave reflection into the flume.

Figure 3 shows the mesh, which is composed of a wave propagation zone downstream and upstream of the buoy and a central zone around the buoy. In the wave propagation zone, the mesh is structured and the cell sizes are $L/70$ in the horizontal direction. There are two transition zones to adapt the diminishing of cells in $L/50$ near the wave maker/flume and the end boundary, and e (cell size at the buoy) at the adjacent zone around the buoy. In the vertical direction of the wave propagation zone, there is a region $2H$ high around the free surface at the rest with cell sizes of $H/20$. From this region to the bottom and the top, there is a stretching of the cell size. This configuration follows previously validated and applied ones described in several works, such as Teixeira et al. (2013), Mendonça et al. (2018), Teixeira and Didier (2023), Güths et al., (2022), and Wiener et al. (2022).

The central zone around the buoy has a nonstructured mesh, composed of quadrilaterals, which includes a

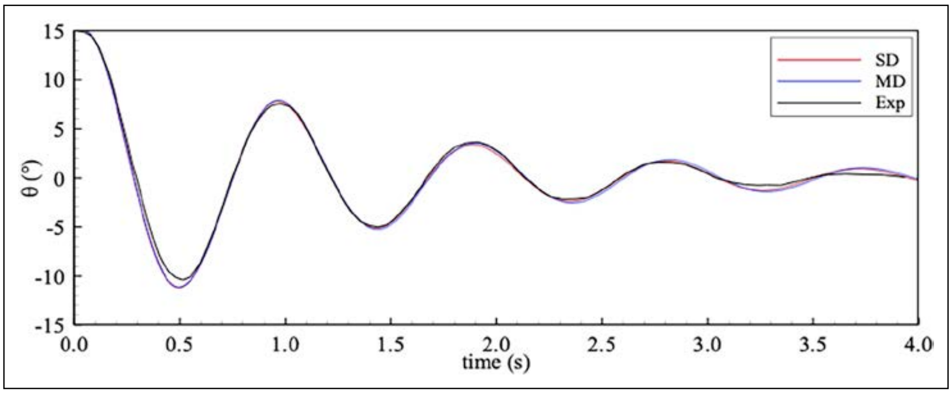

Figure 4. Time series of the angle of rotation of the buoy in the case of buoy decay test.

circular domain defined by a ray of 0.4 m. When the DM method is used, the mesh is deformable in this zone. In the case of the SM method, this circumference is adopted as a slip boundary. The cell size inside the circle, in which the buoy is inserted, is e=1.23 m, defined after a mesh convergence analysis. At the external part of the circumference, cells around the free surface at the rest has sizes equal to e. The cell sizes increase in direction to the bottom (around 2.5 times e) and the top, with higher increasing, since the fluid is the air in this region. This mesh is used in both studied cases.

In the case of the buoy decay, the inclination of 15° is the initial condition about the horizontal direction and the buoy is released to oscillate due to the action of the water buoyancy. Figure 4 shows the time series of the angle of rotation of the buoy by using both SM and DM methods and a comparison with the experimental results of Jung (2004). The amplitude of the angle of rotation diminishes along the time due to the damping caused by both the viscous water forces and the friction on the moving buoy. It can be noticed that the results obtained by both methods are very similar and very close to the experimental one. The oscillation period is the natural period of the system, which is T_N=0.93 s, obtained by the numerical simulations and the experiments.

The second case deals to the incident regular wave, with T=0.93 s and H=0.027 m, over the buoy. Figure 5 shows the time series of the angle of rotation after the stabilization of the flow obtained by both moving methods. It may be emphasized that the buoy oscillates with the same period of the fundamental period of the incident wave. Besides, the clockwise and counterclockwise oscillations have similar behaviors, which is expected since the wave propagates in deep water. Results are compared with experimental ones developed by Jung (2004). It can be observed that both methods present similar results and agree well with the results obtained by experiments.

The maximum and minimum amplitudes of the angle are 11.6° and -11.7°, respectively, for the SM method and 11.4° and -11.4° for DM method. These values are very similar to the experimental ones, which are 11.5° e -11.7°, respectively. Therefore, in terms of accuracy, both methods show a very good performance.

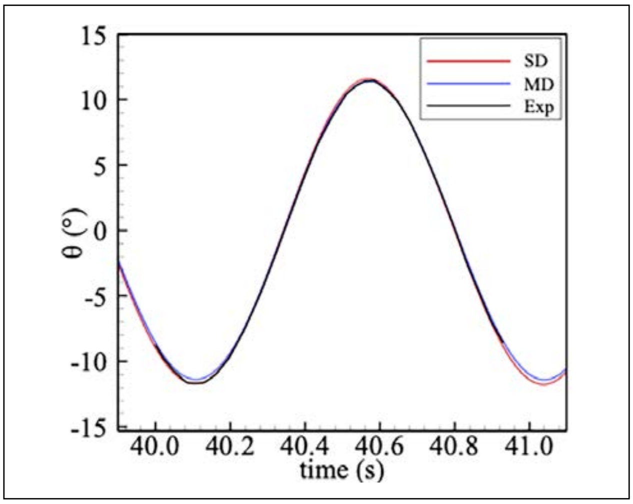

Figure 5. Time series of the angle of rotation of the buoy subjected to an incident regular wave with T=0.93 s and H=0.027 m.

In the case of the DM method, it is very important to analyze the mesh quality. Figure 6 shows the orthogonal quality index to the cells that belongs the zone in which the mesh deforms. It can be noticed that the orthogonal quality index before the mesh deformation (Fig. 6a) is very good (0.70–0.95) to excellent (0.95–1.00), according to ANSYS (2015). It indicates that distortions in the cells are not significant. Besides, even in the maximum amplitude of the angle of rotation of the buoy (Fig. 6b), the distortions of cells are not significant and orthogonal quality index is also very good (0.70–0.95) to excellent (0.95–1.00).

Another important criterion to evaluate the performance of each type of moving method is related to the computation cost. The simulation by using the DM method demands 1.44 and 1.32 times the computational time obtained by the SM method for the free decay test and the incident regular wave over the buoy, respectively. Therefore, considering that both methods present similar accuracy, the SM method is the most suitable for cases with similar characteristics to the buoy one, due to its lower computational cost. It is important to emphasize that, in these cases, the use of the remeshing technique was not necessary, since the distortions of the mesh due to the movement of the buoy were not significant. In

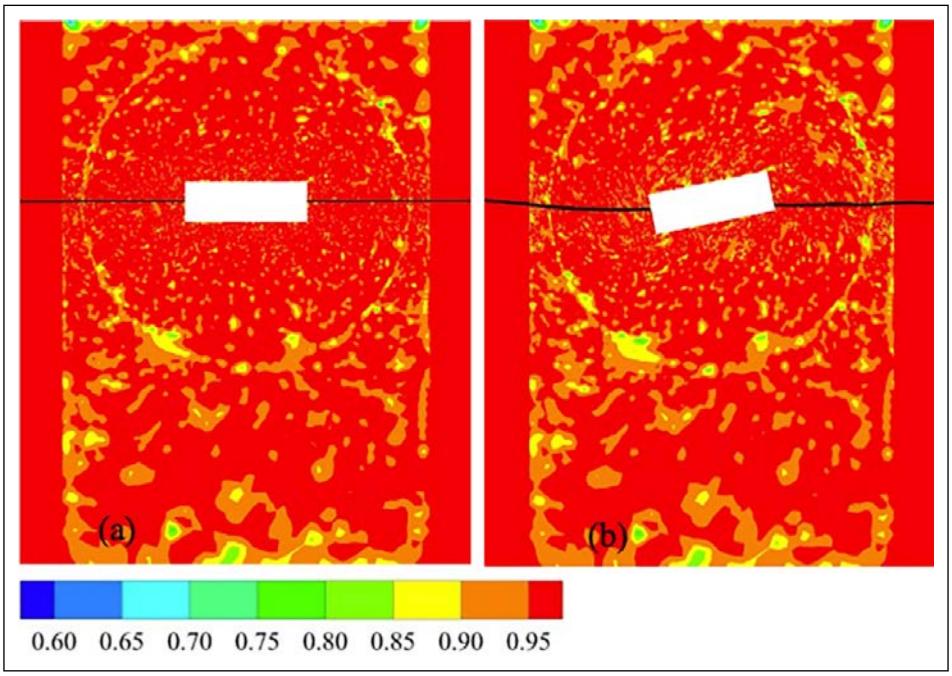

Figure 6. Orthogonal quality index of the cells at (a) the initial condition and (b) the maximum angle of rotation for the incident wave over the buoy using the DM method.

DM: Dynamic mesh.

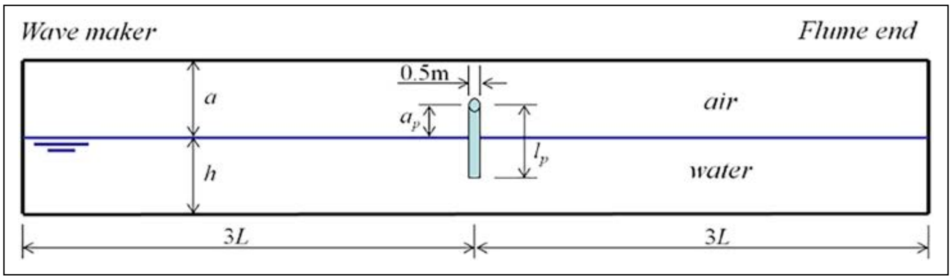

Figure 7. Sketch of the computational domain for the incident wave over the Pendulor device.

cases in which the remeshing technique must be used, the computational time increases and, consequently, this criterion must be re-evaluated.

3.2. Pendulor device

Figure 7 shows the sketch of the computational domain for the case of the incident regular wave over the Pendulor device. The flap of the device with thickness of 0.5 m, and length l_p=7 m, in which 2 m are immersed (a_p), is located at the center of the flume *6L* long and h=10 m deep. The hinge is located at the emerged tip of the flap, which has a specific mass of 1450 kg/m^3 and a mass moment of inertia of I=81667 kg.m^2. In the wave maker, a second order Stokes regular wave is generated with T=12 s and H=1.5 m.

Generally, in this type of device, a hydraulic system is responsible to absorb the mechanical energy (Power take-off, PTO), in which reaction forces of cylinders cause a damping moment (M_{PTO}). In this work, the viscous damping model is used to represent this moment, as follows:

$$M_{PTO} = c_{PTO}\,\dot{\theta} \tag{9}$$

where c_{PTO} is the viscous damping coefficient of the hydraulic system, which is 500 kNms/rad in this study. The mean time mechanical power absorbed by the device is given by

$$P_{PTO} = \frac{1}{T}\int_0^T M_{PTO}\,\dot{\theta}\,dt \tag{10}$$

Figure 8 shows the mesh whose configuration is similar to the buoy case, with two zones of wave propagation and a central zone that includes the flap. The mesh of the central zone around the flap is a non-structured one, composed of quadrilaterals with a minimal edge size of 0.062 m (chosen after a mesh convergence analysis) located at the plate boundary and in the region around the free surface. The cell size increases in direction to the bottom and the top flume, with a similar configuration to the previous case. In the case of the SM method, there is a moving circumference that follows the movement of the device and slips on a circumference coupled to the static mesh. When the DM method is used, the mesh is deformable in the central zone.

Figure 9 shows the velocity magnitude and the stream lines in a region around the flap for a stabilized periodic flow at four

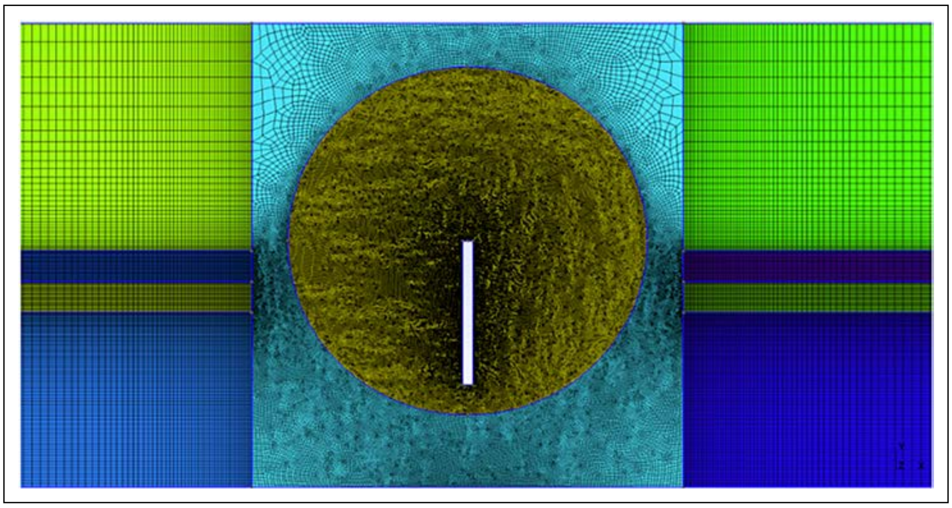

Figure 8. Mesh around the flap.

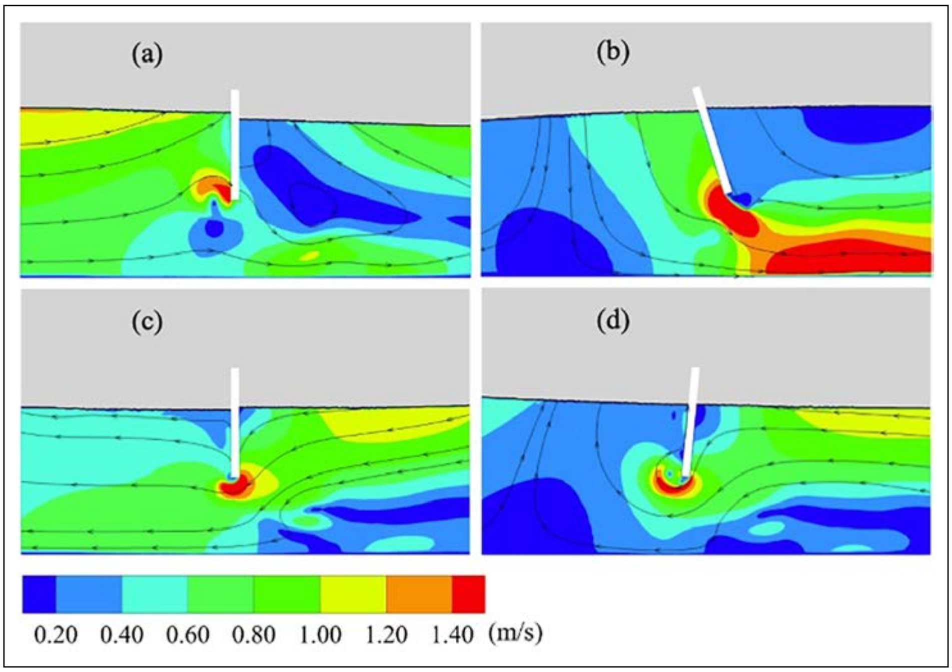

Figure 9. Velocity magnitude and stream lines around the flap using SM method. (a) In the vertical position and moving counterclockwise, (b) in the maximum angle of rotation, (c) in the vertical position and moving clockwise, and (d) in the minimum angle of rotation.

SM: Sliding mesh.

instants by using the SM method: a) in the vertical position and moving counterclockwise, b) in the maximum angle of rotation, c) in the vertical position and moving clockwise, and d) in the minimum angle of rotation. It can be observed that the fluid dynamics is significant around the submerged tip of the flap at every instant. At the instant b), a high velocity intensity can be noted near the tip of the flap and also over a wide area near the bottom of the flume at the rear of the flap. Besides, the emerged tip of the flap is high enough to avoid overtopping due to this incident wave. These results are very similar to the ones obtained using DM method.

Figure 10 shows comparisons of the time series of the angle of rotation, angular velocity, and angular acceleration obtained by both methods. It can be noticed that the time series of both moving methods are very similar. The higher difference is observed in the angular acceleration, which presents a significant non-linear behavior. The angle of rotation oscillates with the predominant frequency equal to the fundamental frequency of the incident wave. The amplitudes counterclockwise, corresponding to the horizontal displacement in the wave propagation direction, are 16.85° and 17.02° for SM and DM, respectively. These values are higher than the amplitudes clockwise, which are 5.26° and 4.61°, respectively. It is expected since the wave propagates on the flume in intermediate water. The angular velocity also has higher amplitudes counterclockwise and shows a higher non-linearity than the angle of rotation. The angular velocity amplitudes counterclockwise and clockwise are 0.130 and

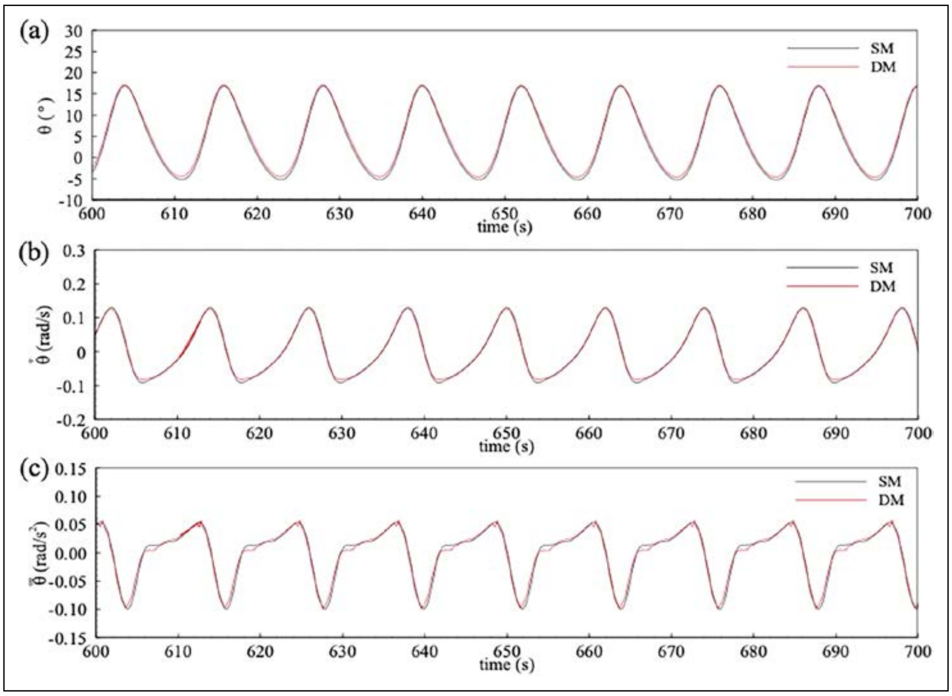

Figure 10. Time series of the (a) angle of rotation, (b) angular velocity and (c) angular acceleration for the Pendulor device.

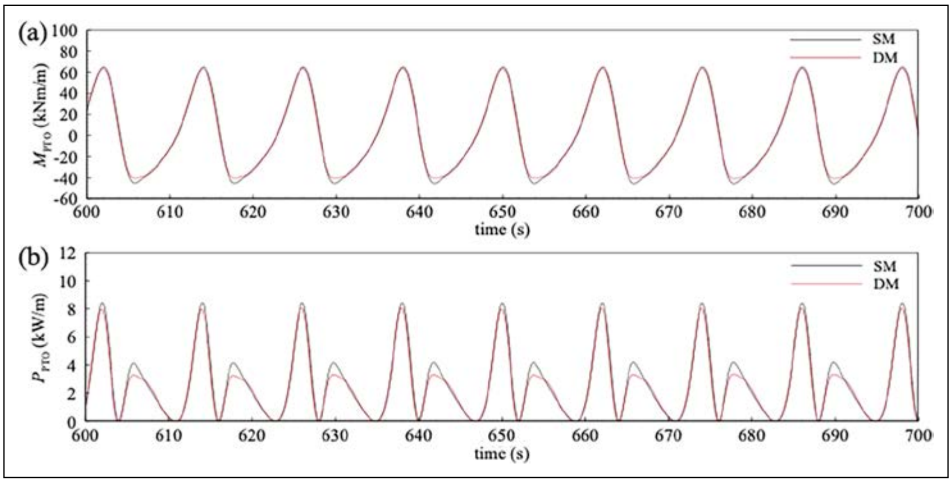

Figure 11. Time series of (a) damping moment and (b) absorbed power for the Pendulor device.

0.091 rad/s, respectively for the DM method and 0.127 and 0.082 rad/s for the SM method. The angular acceleration has also its predominant frequency equal to the one of the incident wave, although other frequencies are observed significantly. Although small differences between both methods are observed in these time series, the general behaviors are similar.

Figure 11 shows the time series of the damping moment (MPTO) and the absorbed power (PPTO) of the device. The results obtained by using SM and DM are similar, with little differences, mainly around the maximum amplitudes clockwise. The damping moment, which directly depends on the angular velocity of the flap, shows a behavior with oscillation predominantly in the fundamental frequency of the incident wave. The amplitudes counterclockwise are 64.91 and 63.37 kNm/m for SM and DM, respectively, which are higher than those clockwise, 45.81 and 40.88 kNm/m, respectively. The absorbed power is higher during the counterclockwise than the clockwise, following the behavior of the angular velocity and the damping moment. The power amplitudes counterclockwise are 8.43 and 8.04 kW/m for SM and DM, respectively, and 4.20 and 3.35 kW/m clockwise. The temporal mean absorbed powers are 2.69 and 2.55 kW/m for SM and DM, respectively, whose differences are about 5%.

Figure 12 shows the orthogonal quality index around the flap by using the DM method before and after the mesh deformation at the maximum angle of rotation counterclockwise. It can be observed that the initial non-structured mesh has a very good index. When the flap is positioned at the maximum angle of rotation, the orthogonal quality remains good. However,

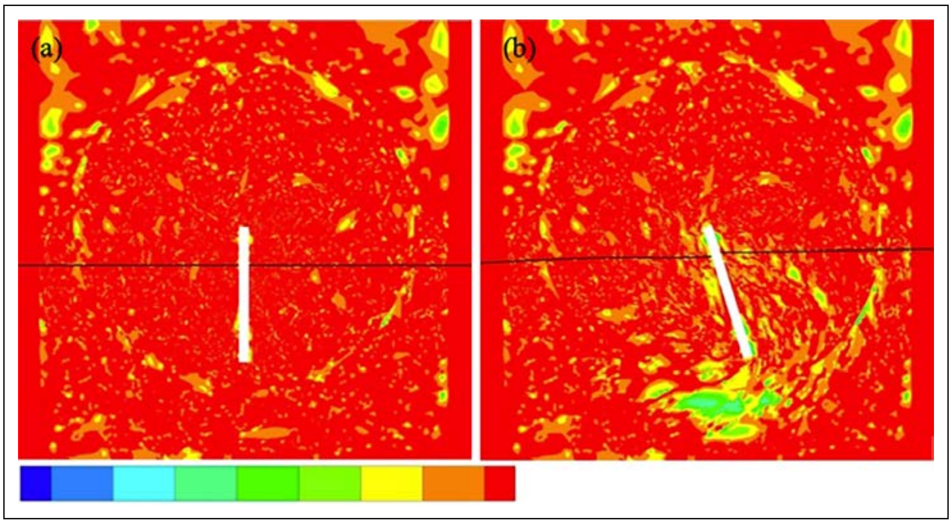

Figure 12. Orthogonal quality index in (a) the initial condition and (b) in the maximum angle of rotation for the case of the Pendulor device using the DM method.

DM: Dynamic mesh.

some distortions are noticed between the tip of the flap and the bottom since the bottom imposes a fixed movement condition on the mesh. It can be emphasized that excessive cell distortions can cause a loss of accuracy.

The computational time demanded by the DM method is 1.29 times the one of the SM method, which confirms the same tendency of the buoy case. This point is a very important criterion for deciding the best moving method to be used. In this case, as in the buoy one, the cell distortions were not large enough to use the remeshing method. If remeshing method was used, probably, the computational time of the DM method would be higher.

4. CONCLUSON

This study showed a numerical analysis of the performance of two moving mesh methods, Sliding Mesh (SM) and Dynamic Mesh (DM), to deal with fluctuating structures with a rotational DOF. The ANSYS Fluent® software, based on the Navier-Stokes equations, was used for free surface flow simulations. Two cases were studied: a buoy and a Pendulor-type wave energy converter.

In the case of the buoy, two analyses were carried out: the free decay test and the action of an incident regular wave over the buoy. The time series of the angle of rotation of the buoy obtained numerically were compared with those obtained by experiments of Jung (2004). Both methods presented a very good accuracy, with similar results to the experimental ones. In the case of the DM method, the orthogonal quality index was very good, even in zones with larger distortions. However, this method presented 1.32 to 1.44 times the computational time of the SM method for the free decay test and the action of an incident regular wave over the buoy, respectively.

In the case of the Pendular-type wave energy converter, the time series of the angle of rotation, angular velocity, angular acceleration, damping moment, and absorbed power of the flap were analyzed. Some low differences were found, mainly in the absorbed power during the rotation counterclockwise. The difference in the mean time absorbed power between both moving methods was about 5%. The computational time of the DM method was 1.29 times the one of the SM method.

This study showed that both moving methods, Sliding Mesh and Dynamic Mesh, have good accuracy to deal with problems that involve semi-submerged structures with a rotational DOF in a plane subjected to incident waves. However, the SM method has the advantage that it requires a lower computational time.

ACKNOWLEDGEMENTS

The authors thank the cooperation between Universidade Federal do Rio Grande – FURG and Laboratório Nacional de Engenharia Civil – LNEC. The first author thanks the scholarship of CNPq. The second author thanks CNPq (307546/2921-7) and FAPERGS (21/2551-0002014-8).

DATA AVAILABILITY STATEMENT

The published publication includes all graphics and data collected or developed during the study.

CONFLICT OF INTEREST

The author declared no potential conflicts of interest with respect to the research, authorship, and/or publication of this article.

ETHICS

There are no ethical issues with the publication of this manuscript.

USE OF AI FOR WRITING ASSISTANCE

No AI technologies utilized.

FINANCIAL DISCLOSURE

The authors declared that this study has received no financial support.

REFERENCES

Amini, E., Nasiri, M., Pargoo, N.S., Mozhgani, Z., Golbaz, D., Baniesmaeil, M., Nezhad, M.M., Neshat, M., Garcia, D.A., & Sylaios, G. (2023). Design optimization of ocean renewable energy converter using a combined Bi-level metaheuristic approach. Energy Conversion and Management: X, 19, Article 100371. [CrossRef]

Anbarsooz, M., Passandideh-Fard, M., & Moghiman, M. (2014). Numerical simulation of a submerged cylindrical wave energy converter. Renewable Energy, 64, 132–143. [CrossRef]

ANSYS (2015). Lecture 7: Mesh quality & advanced topics. 15.0 Release.

ANSYS Fluent® (2016). User's Guide. ANSYS Inc.

Benek, J., Steger, J., & Dougherty, F. (1983). A flexible grid embedding technique with application to the euler equations. In Proceedings of the 6th Computational Fluid Dynamics Conference Danvers, American Institute of Aeronautics and Astronautics. [CrossRef]

Benites-Munoz, D., Huang, L., & Thomas, G. (2024). Optimal array arrangement of oscillating wave surge converters: An analysis based on three devices. Renewable Energy, 222, Article 119825. [CrossRef]

Calderer, A., Seokkoo, & K., Sotiropoulos F. (2014). Level set immersed boundary method for coupled simulation of air/water interaction with complex floating structures. Journal of Computational Physics, 277, 201–227. [CrossRef]

Causon, D., Ingram, D., Mingham, C., Yang, G., & Pearson, R. (2000). Calculation of shallow water flows using a cartesian cut cell approach. Advances in Water Resources, 23, 545–562. [CrossRef]

Didier, E., Teixeira, P. R. F., & Neves M. G. (2017). A 3D numerical wave tank for coastal engineering studies. Defect Diffusion Forum, 372, 1–10. [CrossRef]

Didier, E., & Teixeira, P.R.F. (2022). Validation and comparisons of methodologies implemented in a RANS-VoF numerical model for applications to coastal structures. Journal of Marine Science and Engineering, 10, Article 1298. [CrossRef]

Elhanafi, A., Fleming, A., Leong, Z., & Macfarlane, G. (2016). Effect of RANS-based turbulence models on nonlinear wave generation in a two-phase numerical wave tank. Progress in Computational Fluid Dynamics, 17(3), 141–158. [CrossRef]

Elhanafi, A., Macfarlane, G., Fleming, A., & Leong, Z. (2017). Experimental and numerical investigations on the intact and damage survivability of a floating-moored oscillating water column device. Applied Ocean Research, 68, 276–292. [CrossRef]

Ghasemi, A., Anbarsooz, M., Malvandi, A., Ghasemi, A., & Hedayati, F. (2017). A nonlinear computational modeling of wave energy converters: A tethered point absorber and a bottom-hinged flap device. Renewable Energy, 103, 774–785. [CrossRef]

Gunawardane, S.P., Kankanamge, C.J., & Watabe, T. (2016). Study on the performance of the "pendulor" wave energy converter in an array configuration. Energies, 9(4), Article 282. [CrossRef]

Güths, A. K., Teixeira, P. R. F., & Didier, E. (2022). A Novel Geometry of an Onshore Oscillating Water Column Wave Energy Converter. Renewable Energy, 201, 938–949. [CrossRef]

Hirt, C.W., & Nichols, B.D. (1981). Volume of fluid (VoF) method for the dynamics of free boundaries. Journal of Computational Physics, 39, 201–225. [CrossRef]

Jung, K.H. (2004). Experimental study on rectangular barge in beam sea [Doctoral dissertation]. Texas A&M University.

Ko, S. H., Kim, D., Poguluri, S. K., Cho, I., & Bae, Y. H. (2020). Optimal performance studies of a horizontal eccentric cylinder-type WEC in western sea of Jeju island with linear inviscid and nonlinear viscous numerical model. Ocean Engineering, 202, Article 107180. [CrossRef]

Li, S., & Teng, B. (2021). Fluid resonance between twin floating barges with roll motion under wave action. China Ocean Engineering, 35(6), 789–801. [CrossRef]

Lin, P., & Liu, PL-F. (1998). A numerical study of breaking waves in the surf zone. Journal of Fluid Mechanics, 359, 239–264. [CrossRef]

Luan, Z., Chen, B., Jin, R., He, G., Ghassemi, H., & Jing, P. (2024). Validation of a numerical wave tank based on overset mesh for the wavestar-like wave energy converter in the South China sea. Energy, 290, Article 130192. [CrossRef]

Mendonça, A., Dias, J., Didier, E., Fortes, C.J.E.M., Neves, M.G., Reis, M.T., Conde, J.M.P., Poseiro, P., & Teixeira, P.R.F. (2018). An integrated tool for modelling OWC-WECs in vertical breakwaters: preliminary developments. Journal of Hydro-environment Research, 19, 198–213. [CrossRef]

Menter, F.R. (1994). Two-equation eddy-viscosity turbulence models for engineering applications. AIAA Journal, 32, 1598–1605. [CrossRef]

Penalba, M., Davidson, J., Windt, C., & Ringwood, J. V. (2018). A high-fidelity wave-to-wire simulation platform for wave energy converters: coupled numerical wave tank and power take-off models. Applied Energy, 226, 655–669. [CrossRef]

Peric, M., & Ferziger, J. H. (1997). Computational Methods for Fluid Dynamics. 2nd ed., Springer, Berlin.

Schlichting, H. (1979). Boundary-layer theory. McGraw-Hill.

Sharma, N., & Patankar, N.A. (2005). A fast computation technique for the direct numerical simulation of rigid particulate flows. Journal of Computational Physics, 205, 439–57. [CrossRef]

Schmitt, P., & Elsaesser, B. (2015). On the use of OpenFOAM to model oscillating wave surge converters. Ocean Engineering, 108, 98–104. [CrossRef]

Teixeira, P.R.F., Davyt, D.P., & Didier, E., Ramalhais R. (2013). Numerical simulation of an oscillating water column device using a code based on Navier Stokes equations. Energy, 61(1), 513–530. [CrossRef]

Teixeira, P.R.F., Didier, E., & Neves, M.G. (2017). A 3D RANS-VOF wave tank for oscillating water column device studies. In Proceedings VII International Conference on Computational Methods in Marine Engineering, MARINE 2017, Nantes, France, 710–721.

Teixeira, P.R.F., & Didier, E. (2023). Numerical analysis of performance of an oscillating water column wave energy converter inserted into a composite breakwater with rubble mound foundation. Ocean Engineering, 278, Article 114421. [CrossRef]

Wei, Y., Yu, S., Li, X., Zhang, C., Ning, D., & Huang, L. (2024). Hydrodynamic analysis of a heave-hinge wave energy converter combined with a floating breakwater. Ocean Engineering, 293, Article 116618. [CrossRef]

Wei, Y., Rafiee, A., Henry, A., & Dias, F. (2015). Wave interaction with an oscillating wave surge converter, Part I: viscous effects. Ocean Engineering, 104, 185–203. [CrossRef]

Westphalen, J., Greaves, D.M., Raby, A., Hu, Z.Z., Causon, D.M., Mingham, C.G., Omidvar, P., Stansby, P.K., & Rogers, B.D. (2014). Investigation of wave-structure interaction using state of the art CFD techniques. Open Journal of Fluid Dynamics, 4, 18–43. [CrossRef]

Windt, C., Davidson, J., & Ringwood, J. V. (2018). High-fidelity modelling of ocean wave energy systems: A review of computational fluid dynamics-based nuerical wave tanks. Renewable ans Sustainable Energy Reviews, 93, 601–630. [CrossRef]

Wiener, G.F., Teixeira, P.R.F., & Didier, E. (2022). Numerical evaluation of optimal sizes of Wells turbine and chamber of a cluster of Oscillating Water Columns integrated into a breakwater on the Southern Brazilian Coast. Journal of Waterway, Port, Coastal, and Ocean Engineering, 148(4), Article 04022009. [CrossRef]